

This article was downloaded by:

On: 16 January 2011

Access details: *Access Details: Free Access*

Publisher *Taylor & Francis*

Informa Ltd Registered in England and Wales Registered Number: 1072954 Registered office: Mortimer House, 37-41 Mortimer Street, London W1T 3JH, UK



Journal of Energetic Materials

Publication details, including instructions for authors and subscription information:

<http://www.informaworld.com/smpp/title~content=t713770432>

Numerical modeling of projectile impact shock initiation of bare and covered composition-B

John Starkenberg^a; Yun Huang^a; Alvin Arbuckle^a

^a Ballistic Research Laboratory AMCCOM Aberdeen Proving Ground, Maryland

To cite this Article Starkenberg, John , Huang, Yun and Arbuckle, Alvin(1984) 'Numerical modeling of projectile impact shock initiation of bare and covered composition-B', Journal of Energetic Materials, 2: 1, 1 – 41

To link to this Article: DOI: 10.1080/07370658408012327

URL: <http://dx.doi.org/10.1080/07370658408012327>

PLEASE SCROLL DOWN FOR ARTICLE

Full terms and conditions of use: <http://www.informaworld.com/terms-and-conditions-of-access.pdf>

This article may be used for research, teaching and private study purposes. Any substantial or systematic reproduction, re-distribution, re-selling, loan or sub-licensing, systematic supply or distribution in any form to anyone is expressly forbidden.

The publisher does not give any warranty express or implied or make any representation that the contents will be complete or accurate or up to date. The accuracy of any instructions, formulae and drug doses should be independently verified with primary sources. The publisher shall not be liable for any loss, actions, claims, proceedings, demand or costs or damages whatsoever or howsoever caused arising directly or indirectly in connection with or arising out of the use of this material.

NUMERICAL MODELING OF PROJECTILE IMPACT SHOCK INITIATION

OF BARE AND COVERED COMPOSITION-B

John Starckenberg
Yun Huang
Alvin Arbuckle
Ballistic Research Laboratory
AMCCOM
Aberdeen Proving Ground, Maryland

ABSTRACT

This paper concerns our numerical modeling of the projectile impact shock initiation of composition-B (comp-B). We have considered both bare and covered charges impacted by cylindrical steel projectiles using the Los Alamos 2DE code. We have examined the flow fields in some detail and compared predicted critical velocities with published experimental values. For bare charges, we observed two different mechanisms by which the critical velocity is determined. For impacts by projectiles of sufficiently large diameter initiation occurs as the impact induced shock wave builds to detonation by reinforcement due to burning behind the shock. For smaller

Journal of Energetic Materials Vol. 2, 1-41
This paper is not subject to U.S. copyright.
Published in 1984 by Dowden, Brodman & Devine, Inc.

diameter, high velocity projectiles, we saw that detonation or near detonation breaks out immediately on impact, but may be quenched by the ensuing rarefactions. We found that 2DE predicted the critical velocity accurately, We checked $\int p^2 dt$ values along the initiation threshold and found them to be relatively constant. We also simulated the special projectile geometries considered by Moulard, and found that 2DE provided a qualitative explanation of his observations. In the case of covered projectiles we found flow fields similar to the bare charge case. The thickest cover plates allowed the rarefaction to overtake the shock before they entered the explosive and significantly raised the critical velocity. The predicted initiation thresholds agree with Howe's results but not with Slade and Dewey's.

INTRODUCTION

Projectile impact shock initiation of high explosives has long been a subject of interest in the energetic materials community. Considerable experimental data has been generated over the years.¹⁻⁴ Numerical modeling of projectile impact shock initiation for comparison with experiments has been reported in at least one case.⁴ However, only the predicted critical velocities and no detailed analysis of the flow fields revealed by the computations were presented. In another numerical study, Mader and Pimbley⁵ modeled the initiation of

explosives due to the impact of shaped charge jets using the same computer code used in the present paper.

This paper concerns our numerical modeling of the projectile impact shock initiation of composition-B (comp-B). We have considered both bare and covered charges impacted by cylindrical steel projectiles using the Los Alamos 2DE code. HOM equations of state for inert comp-B, reactive comp-B, and 347-steel were used. We have examined the flow fields in some detail and compared predicted critical velocities with published experimental values.

BRIEF DESCRIPTION OF 2DE

The 2DE code⁶ is a two-dimensional, reactive hydrodynamic computer code which makes use of the equations of motion in Eulerian form. It incorporates the HOM equation of state and, most important for our application, the Forest Fire model (giving reaction rate as a function of pressure) for shock initiation of high explosives. In our computations we used an elastic-plastic constitutive model to account for the behavior of steel.

PROJECTILE IMPACT SHOCK INITIATION OF BARE COMPOSITION-B Geometry and Computational Considerations

The axisymmetric geometry used in the bare charge projectile impact computations is illustrated in Figure 1. We have considered cylindrical steel projectiles of unit aspect ratio (l/d) since Brown and Whitbread² have demonstrated that

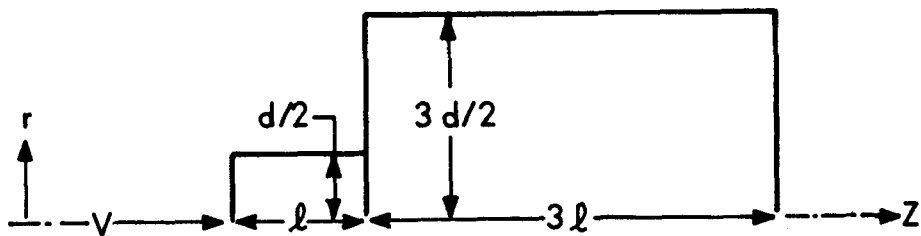


FIGURE 1

Axisymmetric Geometry Used in Projectile Impact Computations

different aspect ratios do not produce different critical velocities for shock initiation, except in the case of thin discs ($l/d < 1/4$). Computations were made for projectile diameters, d , of 4, 5, 8, 10, 12, 15 and 18 mm. Sufficient target material is provided when the length and diameter of the explosive charge are each three times the corresponding projectile dimensions.

We set up these impact problems for 2DE calculation with axisymmetric grids as summarized in Table 1. Here Δr is the radial cell dimension, I the number of cells along the radial axis, Δz the axial cell dimension, J the number of cells along the axis of symmetry, Δt the time step for each computational cycle, and N the total number of cycles to be completed.

TABLE 1

Input Data for 2DE Computational Grids - Bare Charges

d (mm)	$\Delta r, \Delta z$ (mm)	I	J	Δt (μs)	N
4	0.200	40	90	0.005	400
5	0.250	40	70	0.006	400
8	0.207	60	105	0.006	500
10	0.340	60	105	0.010	500
12	0.400	60	105	0.008	500
15	0.500	60	105	0.010	500
18	0.600	60	105	0.010	400

Results

Flow Field Observations. A number of graphical representations of our numerical results are available. The sequence of events in projectile impact shock initiation is most clearly illustrated in the series of mass fraction contour plots of Figure 2. The mass fraction varies from one to zero as chemical reaction in the explosive runs to completion. These plots show results for the impact of a 10 mm diameter projectile at 1.1 km/s, just above the critical velocity. The position of the impact shock is also shown. At 1.0 μ s after impact, burning is observed throughout the region between the shock and the projectile, but detonation has not yet begun. Detonation, which may be recognized by the close spacing of the contour lines, is first observed to break out after the shock has propagated some distance from the impact point. The detonation then spreads outward along the shock and is well established by 1.5 μ s. It also propagates back toward the projectile through the partially reacted material.

Determination of Critical Impact Velocity and Comparison with Experimental Data. By varying impact velocity in computations of this type we were able to determine the critical velocity as a function of projectile diameter. In Figure 3 we have plotted the 2DE results together with the experimental results of Slade and Dewey¹ as well as the Jacobs-Roslund empirical formula³. The agreement is excellent, with the 2DE go and no-go

predictions all bracketing the empirical curve. We have also included the data for ISL comp-B (65/35) reported by Moulard at the last detonation symposium.⁷ This explosive is reported to be generally less sensitive than U.S. comp-B and particularly less sensitive when impacted by small projectiles!

We observed a different mode of critical shock initiation at the smaller diameters. When the projectile diameter is small and the impact velocity is high detonation appears almost immediately on impact as shown in Figure 4 at $0.3 \mu\text{s}$ after the impact of a 4 mm diameter projectile at 1.7 km/s. In this case detonation continues to propagate and a considerable amount of explosive has been consumed by $1.2 \mu\text{s}$. On the other hand, when the impact velocity is reduced to 1.6 km/s, the detonation that breaks out immediately does not continue to propagate but is quenched by the action of following rarefactions as shown in Figure 5. Thus, the mass fraction contour lines begin to spread out by $0.7 \mu\text{s}$. Little or no progress is made between $1.0 \mu\text{s}$ and $1.5 \mu\text{s}$ as the detonation dies out leaving a bubble of detonation products in its wake. It should be noted that these detonations are not overdriven as were those computed by Mader and Pimbley⁵ for shaped charge jet impact. An overdriven detonation in comp-B produced by the impact of a steel projectile would require an impact velocity exceeding approximately 2.8 km/s.

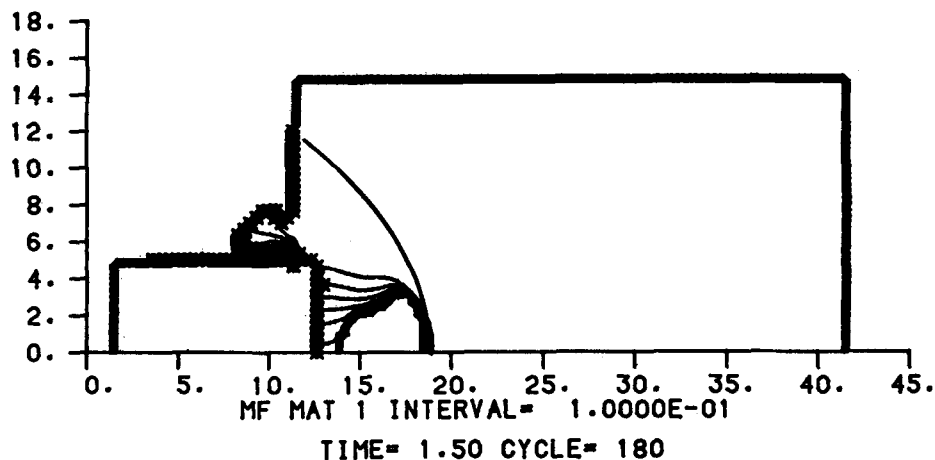
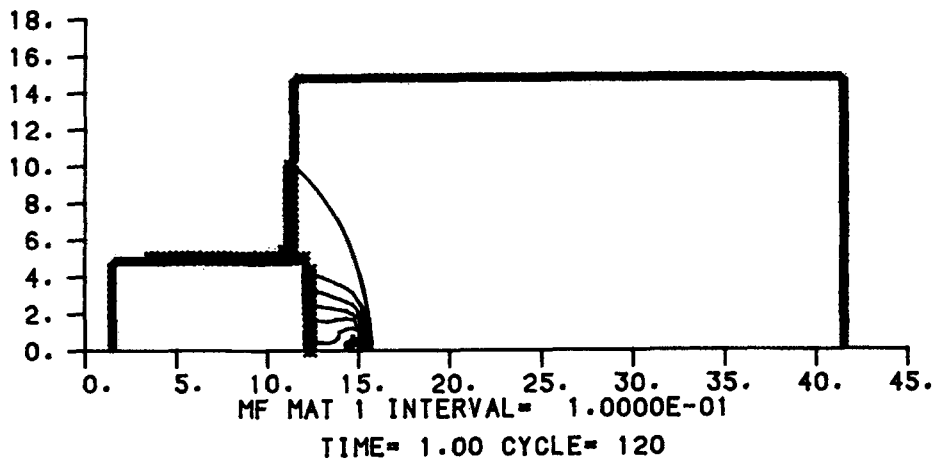


FIGURE 2

Sequence of Mass Fraction Contour Plots for the Supercritical Impact of a 10 mm Diameter Steel Projectile at 1.1 km/s against Bare Composition-B

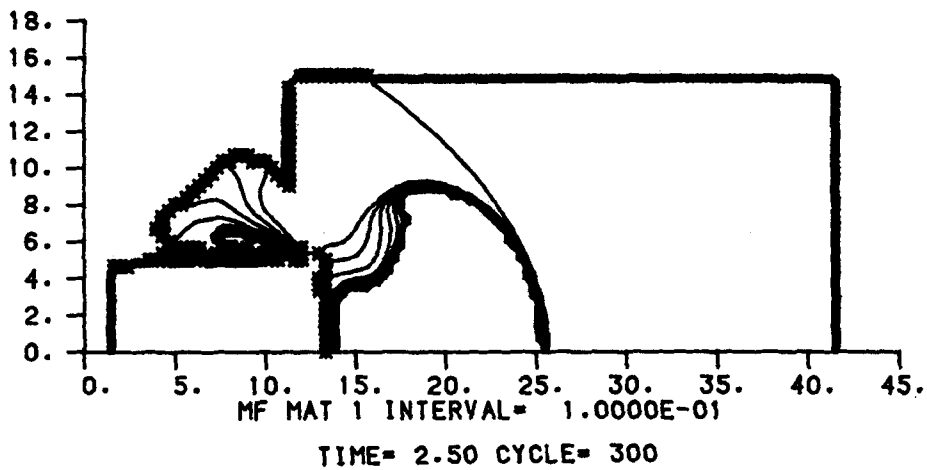
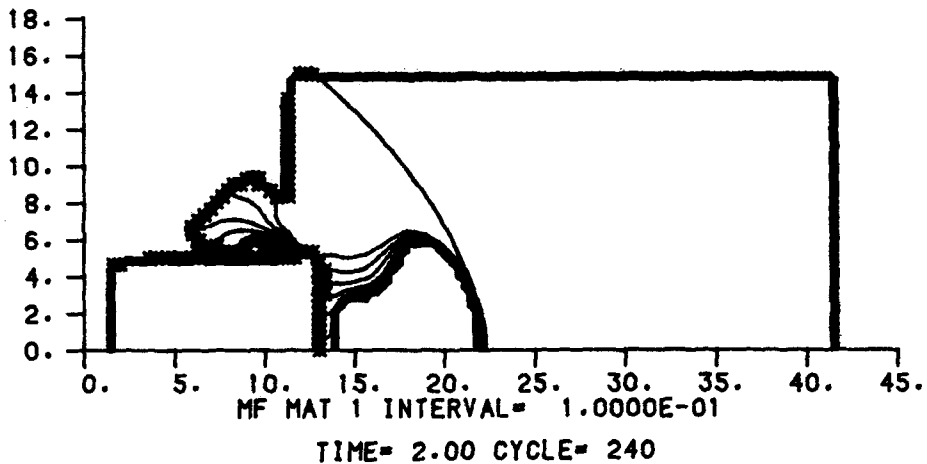


FIGURE 2

(CONT'D)

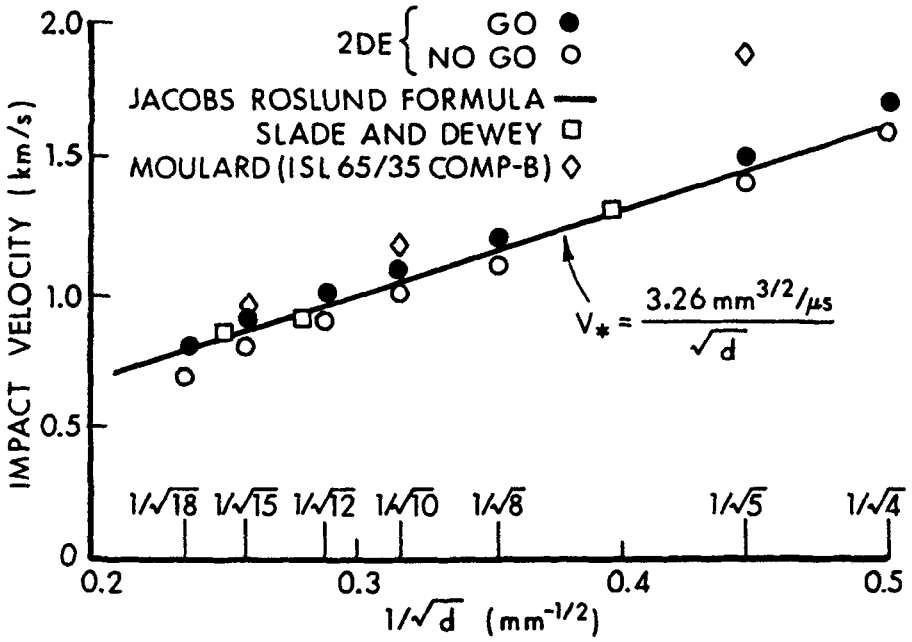


FIGURE 3

Critical Impact Velocity as a Function of Projectile Diameter -
 Comparison of 2DE Predictions with Published Experimental
 Data for Bare Composition-B

Actually, full CJ pressure is never achieved in these detonations. Figure 6 shows a series of pressure and mass fraction profiles along the axis of symmetry at various times for the 4 mm projectile impact at 1.6 km/s. While the mass fraction drops rapidly to zero the pressure never rises above about 23 GPa.

In order to assess the relationship between the 2DE predictions of critical velocity and the critical p^2t concept, we made a series of computations in which the Forest Fire model was deactivated and the explosive treated as an inert material. By observing the pressure history of the target explosive adjacent to the impact point we were able to calculate $\int p^2 dt$. Computations corresponding to our highest subcritical impact velocities for projectile diameters ranging from 5 mm to 18 mm were made. The results, summarized in Table 2, show that, while peak shock pressure decreases with decreasing impact velocity, $\int p^2 dt$ remains fairly constant along the initiation threshold. Thus, the critical p^2t concept appears consistent with Forest Fire.

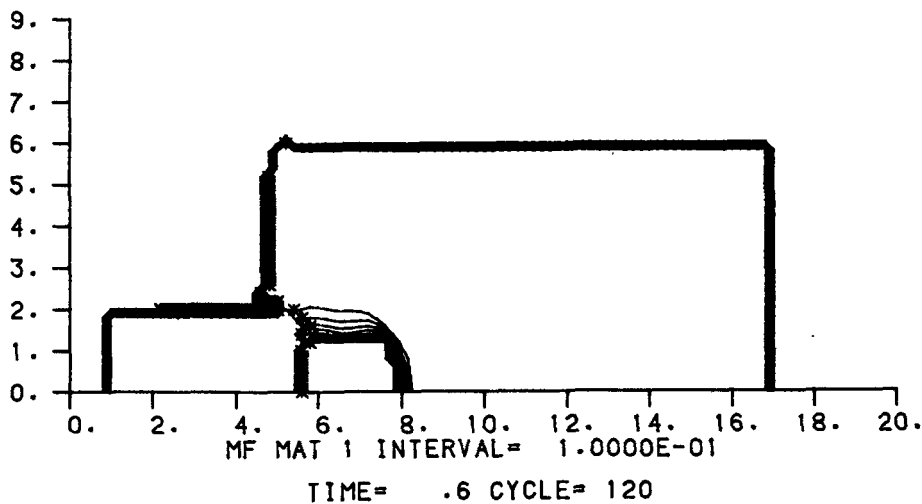
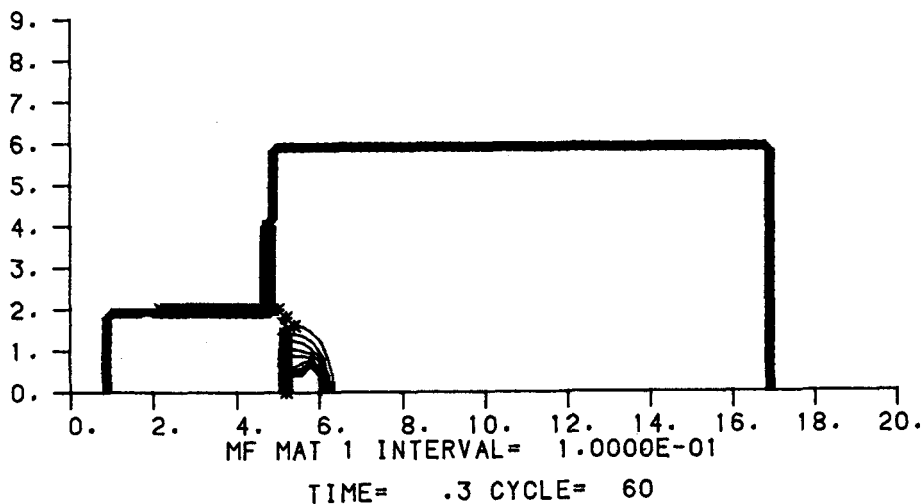


FIGURE 4

Sequence of Mass Fraction Contour Plots for the Supercritical Impact of a 4 mm Diameter Steel Projectile at 1.7 km/s against Bare Composition-B

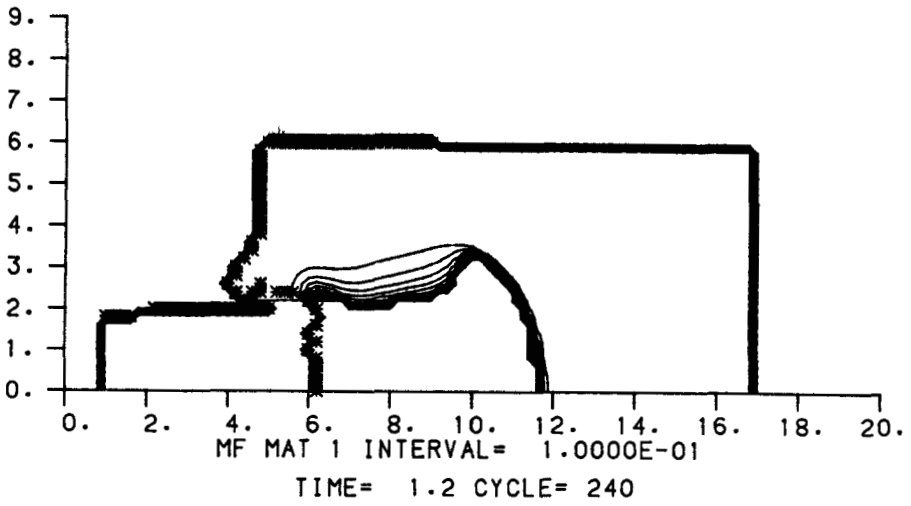
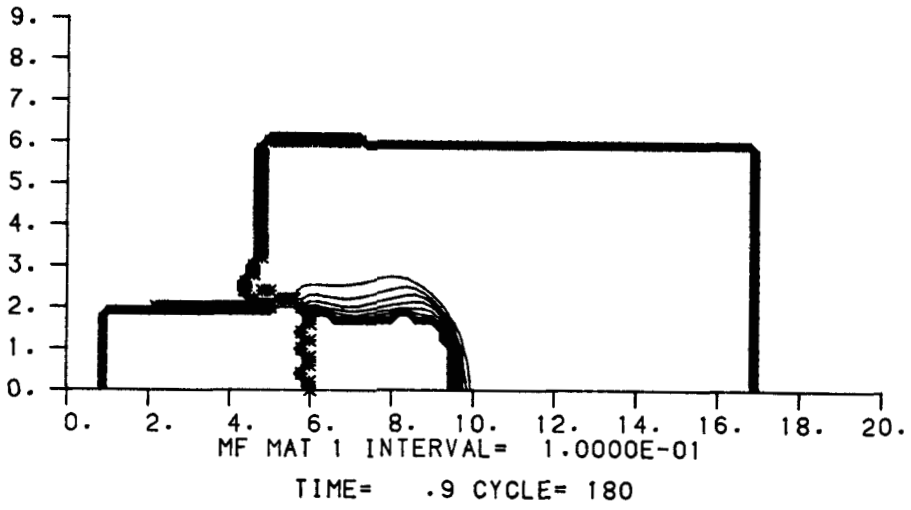


FIGURE 4

(CONT'D)

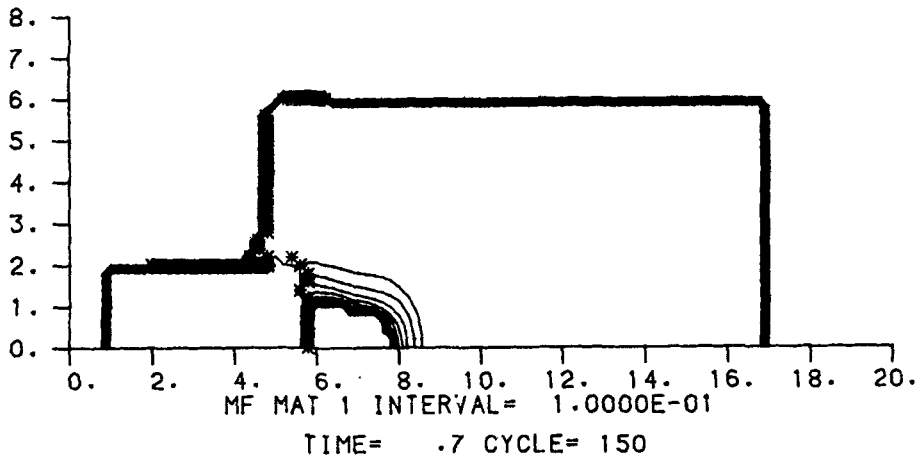
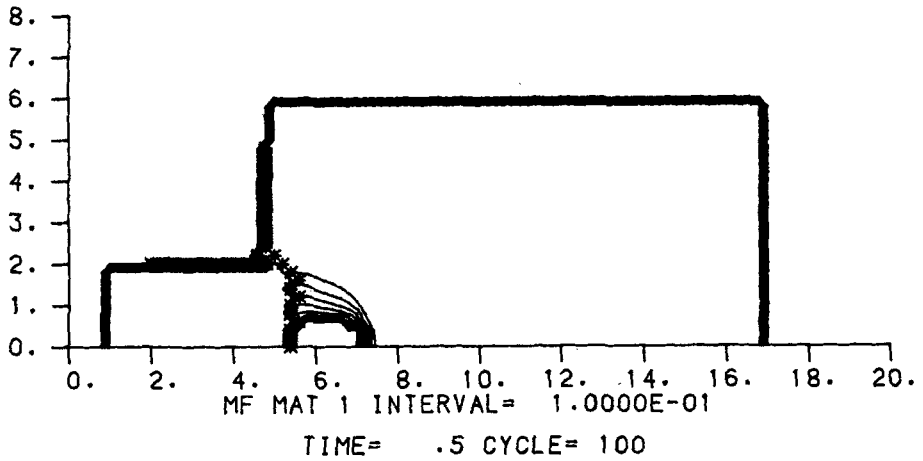


FIGURE 5

Sequence of Mass Fraction Contour Plots for the Subcritical Impact
of a 4 mm Diameter Steel Projectile at 1.6 km/s against Bare
Composition-B

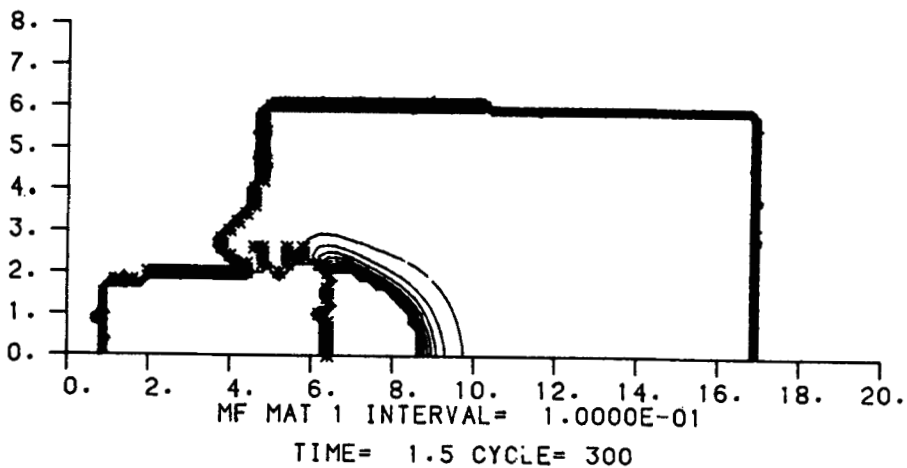
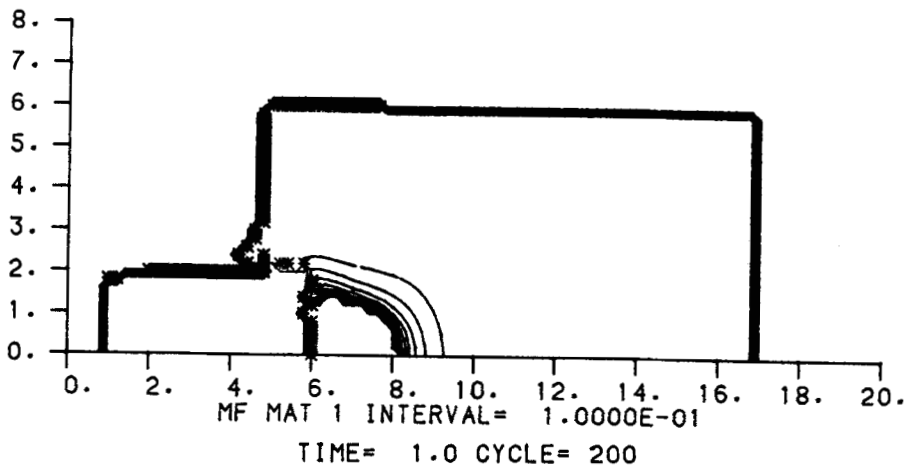


FIGURE 5
(CONT'D)

Downloaded At: 14:10 16 January 2011

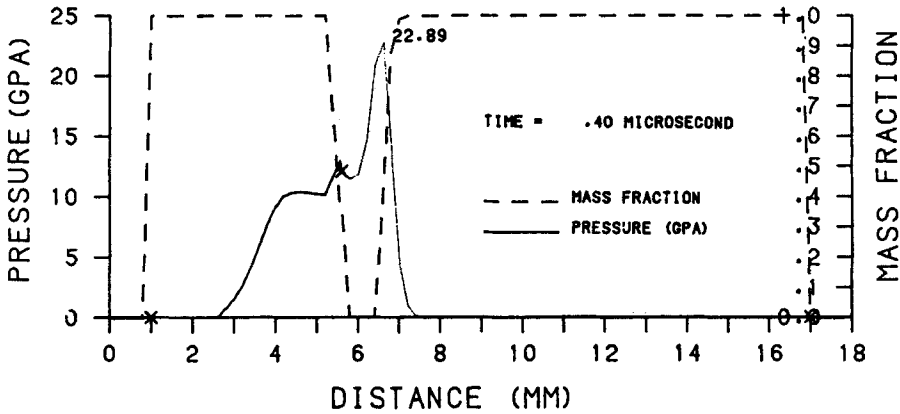
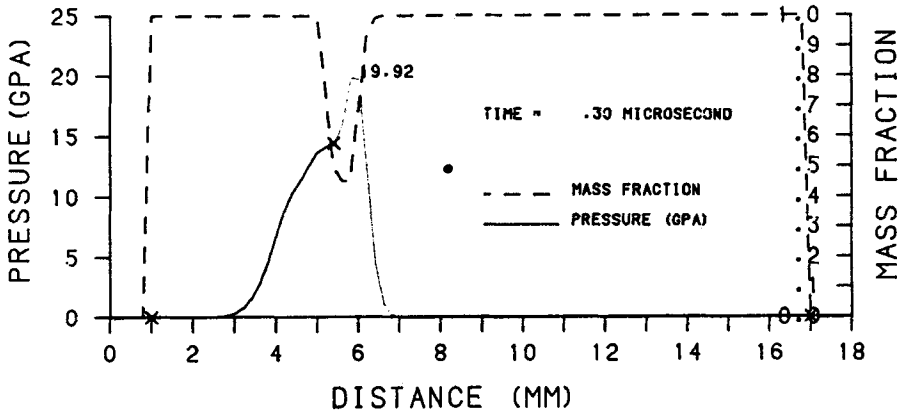


FIGURE 6

Sequence of Pressure and Mass Fraction Profiles for the Subcritical Impact of a 4 mm Diameter Steel Projectile at 1.6 km/s against Bare Composition-B

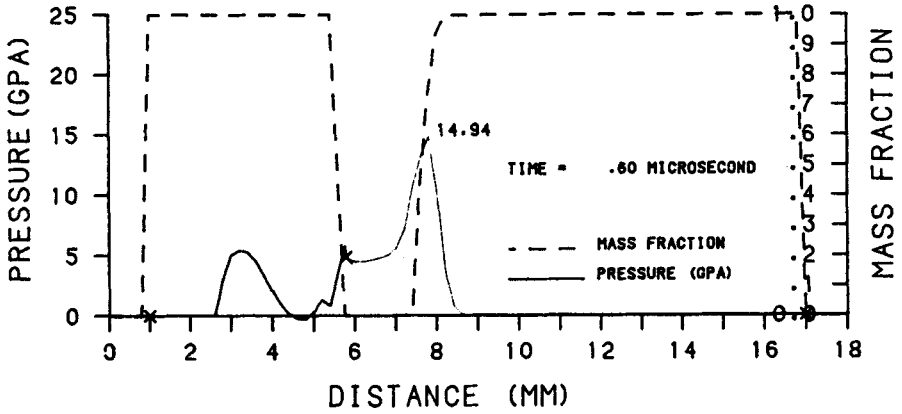
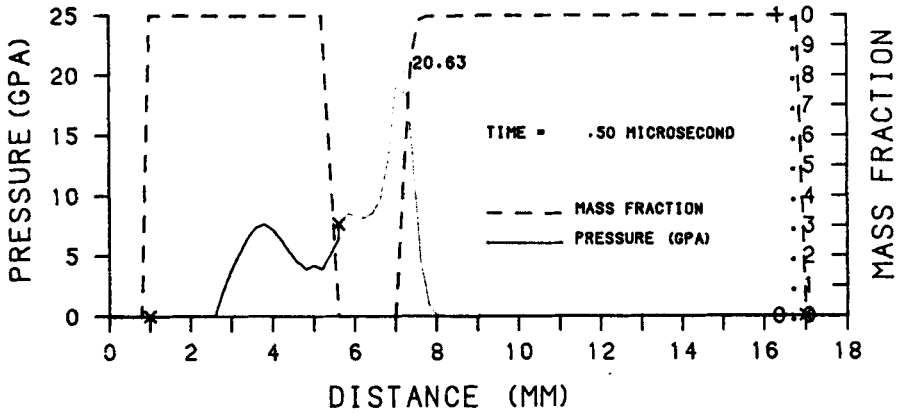


FIGURE 6

(CONT'D)

TABLE 2. Response of "Inert" Composition-B to Critical Projectile Impact

Projectile Diameter (mm)	Impact Velocity (km/s)	Peak Shock Pressure (GPa)	$\int p^2 dt$ (GPa ² - μ s)
5	1.4	9.6	32
8	1.1	7.0	32
10	1.0	6.0	31
12	0.9	5.3	28
15	0.8	4.5	28
18	0.7	3.8	25

Shock to Detonation Transition Paths. The Forest Fire Model is based in part on the single curve buildup hypothesis. Thus, the Pop-plot is interpreted as describing the process of buildup to detonation in the shock pressure - distance to detonation plane. This is true at least for the planar geometries in which single curve buildup has been observed. In an earlier numerical study using 2DE, we had occasion to consider the planar problem arising when a flyer plate of sufficient lateral extent strikes a comp-B target⁸. Once the distance along the axis of symmetry at which steady state detonation first appears has been determined, the progress of shock buildup toward detonation as a function of distance of run to detonation can be compared to the

Pop-plot. This has been done for the problems of 10 mm thick flyer plates striking comp-B targets at 0.6 and 0.7 km/s in Figure 7. The results indicate that 2DE reproduces the single curve buildup phenomenon in the planar geometry. The projectile impact data, however, does not appear to produce a single curve buildup along the axis of symmetry as illustrated in Figure 8.

Special Geometries. At the Seventh Symposium on Detonation, Moulard presented some interesting experimental results in which ISL comp-B was impacted by projectiles of circular, annular and rectangular cross-section.⁷ Although the projectiles were designed to yield the same overall shock duration, he observed considerable differences in the critical velocities produced by each. Specifically he found that the cylindrical projectile required the highest critical velocity (about 2 km/s), the annular projectile required the lowest critical velocity (less than 1 km/s), and the rectangular cross-section produced an intermediate critical velocity. He sought to explain this by introducing a critical area concept. We were interested in determining whether the classical shock initiation concepts incorporated in 2DE could explain these observations without recourse to additional concepts. The circular and annular cross-sections could be represented exactly. Indeed, the circular cross-section computation had already been completed. The impact of a rectangular cross-section projectile is, strictly, a three dimensional problem, but we represented it by

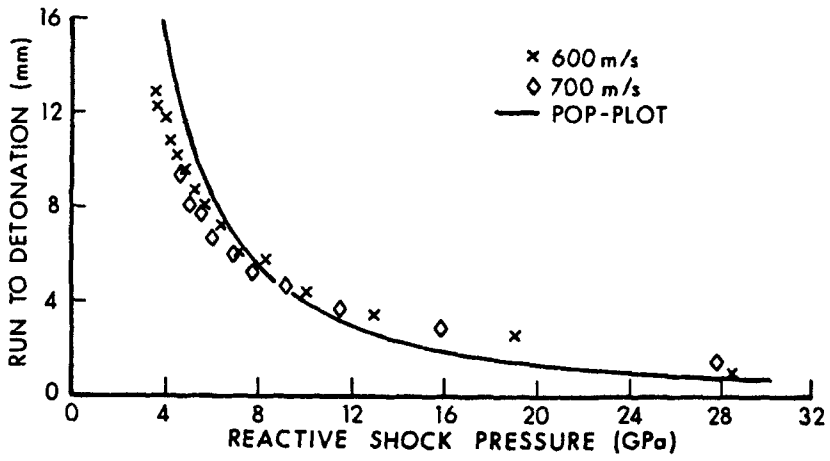


FIGURE 7

Comparison of Computed Paths to Detonation with Pop-plot - Flyer Plate Impact against Bare Composition-B

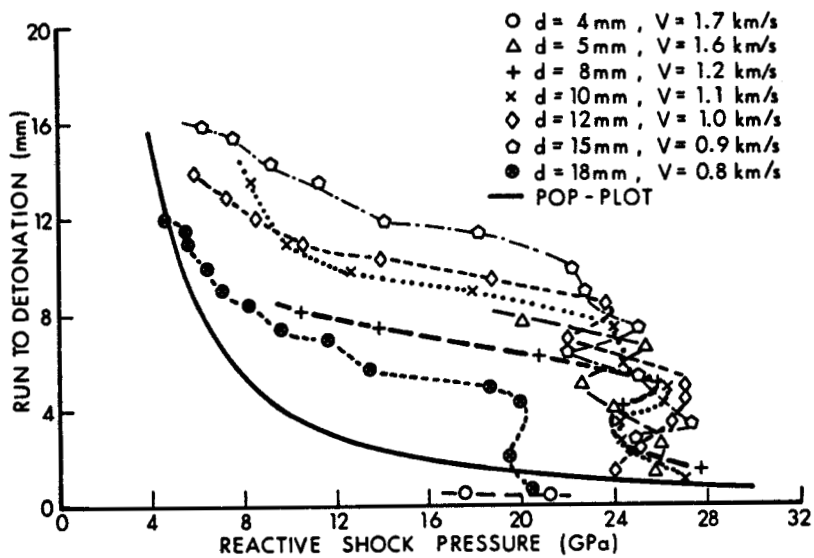





FIGURE 8

Comparison of Computed Paths to Detonation with Pop-plot - Projectile Impact against Bare Composition-B

the impact of a slab of infinite breadth having the thickness of the smallest dimension (5 mm) of the projectile used in the experiments. The experimentally and numerically determined critical velocities are listed in Table 3. The results show that the classical concepts on which the Forest Fire Model is built are sufficient for a qualitative explanation of the Moulard observations. The principal reason for the absence of quantitative agreement is the different formulation of ISL comp-B and its reported lower sensitivity to small diameter projectile impact.

TABLE 3. Comparison of Moulard Experiments with 2DE Simulation.

<u>Projectile</u> <u>Cross-section</u>	<u>Critical Velocity (km/s)</u>	
	<u>Moulard Experiments</u> (65/35 comp-B)	<u>2DE Predictions</u> (60/40 comp-B)
5 mm 	1.95 - 2.02	1.40 - 1.50
5 mm i.d. 15 mm o.d. 	1.06 - 1.11	0.80 - 0.90
5 mm x 11 mm 	1.33 - 1.42	1.10 - 1.15

Some of the reasons for the variations in critical velocity with projectile cross-section become apparent when we observe the flow fields produced. Figure 9 shows a series of mass fraction contour plots for the impact of the annular projectile. The relatively low impact velocity produces no immediate reaction adjacent to the impact point. However, at a later time, shock reflection (probably Mach stem formation) at the axis of symmetry produces higher pressures than the circular cross-section projectile impact at the same velocity. Thus, the detonation is observed to break out along the axis of symmetry at lower impact velocities. Of perhaps greater interest, then, is the difference between the circular and rectangular cross-section results. The only major difference here is the rate at which the rarefaction quenches the incipient detonation. Remember that in the small diameter case we observed immediate detonation which was then quenched by the action of the following rarefaction. The results for the rectangular cross-section are shown in Figures 10 and 11. Figure 10 shows mass fraction contours for a supercritical impact at 1.25 km/s. Detonation arises as a result of shock to detonation transition. In the subcritical impact at 1.10 km/s in Figure 11, no detonation occurs. It remains to be determined whether this strong effect on critical velocity is manifested with projectiles of larger dimensions for which simple shock to

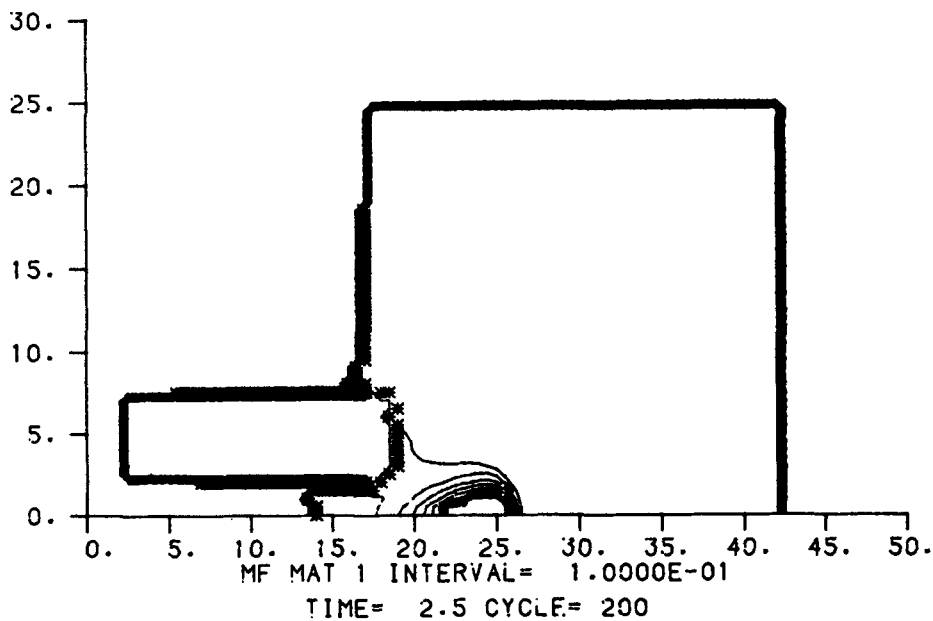
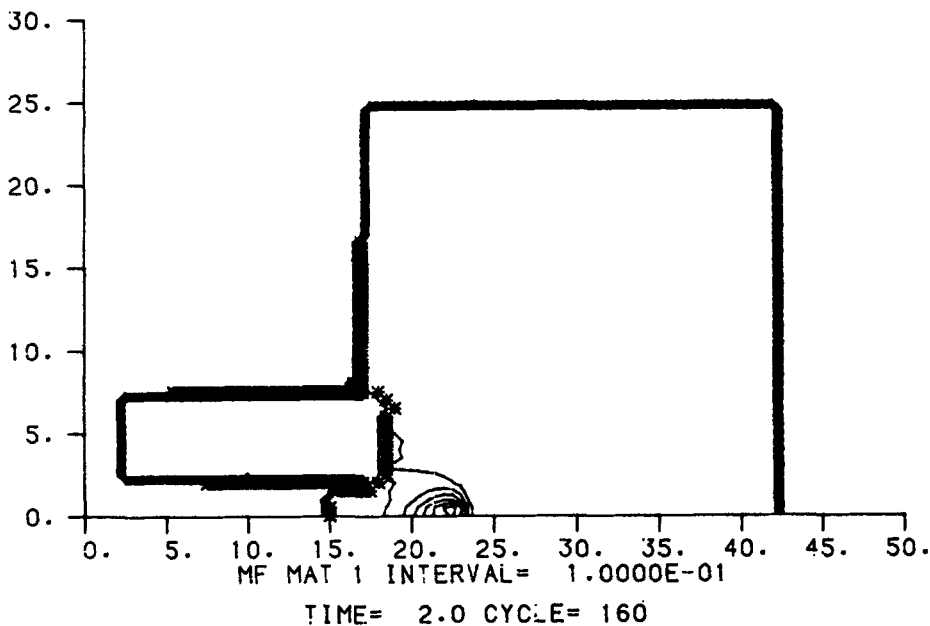


FIGURE 9

Sequence of Mass Fraction Contour Plots for the Supercritical Impact of an Annular Cross-Section Steel Projectile at 0.9 km/s against Bare Composition-B

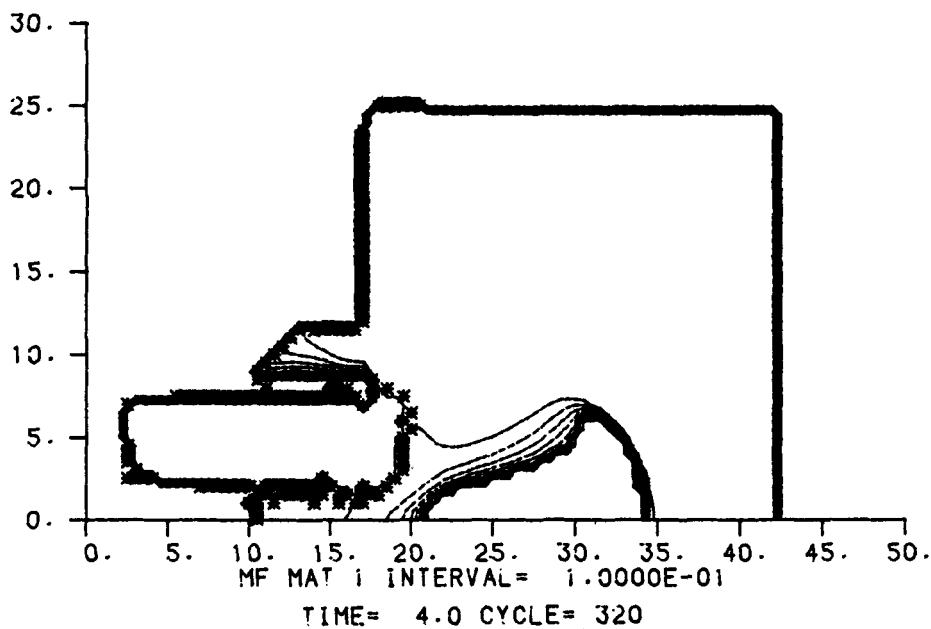
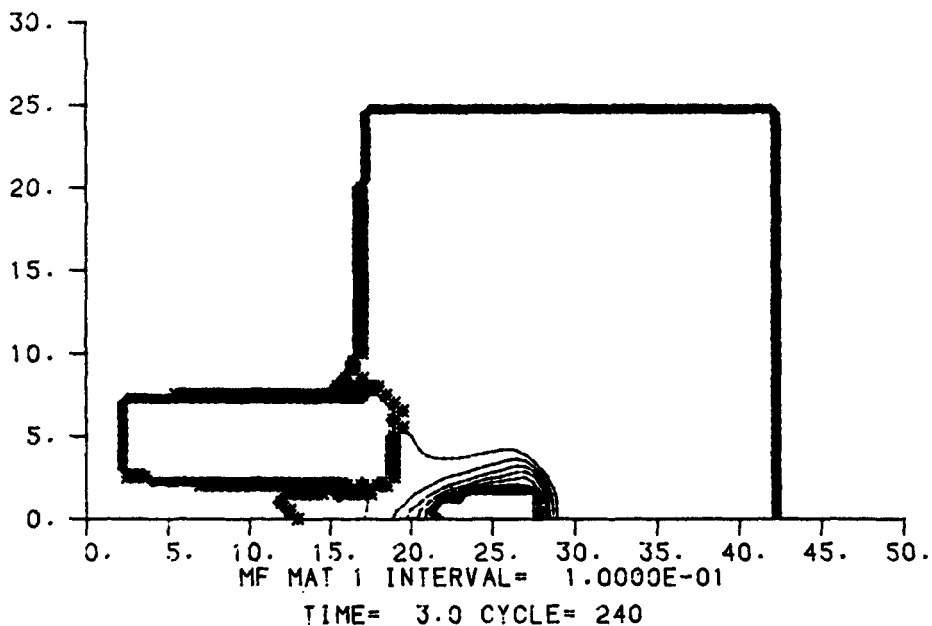


FIGURE 9

(CONT'D)

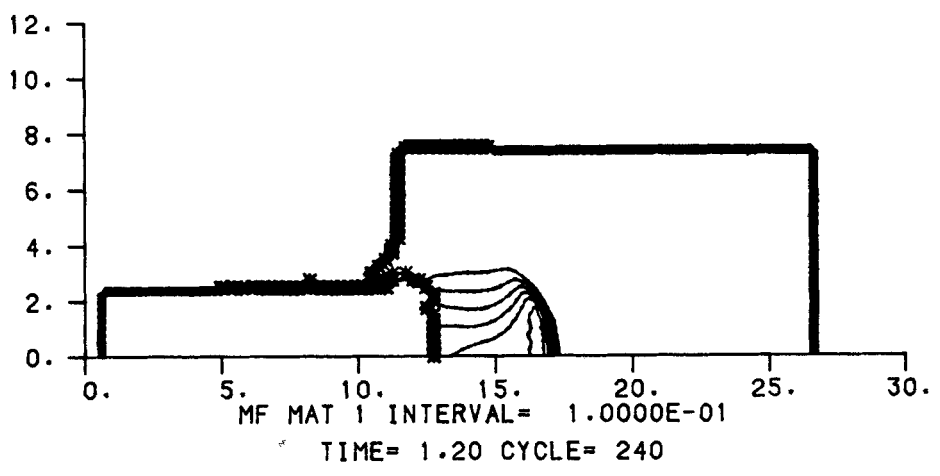
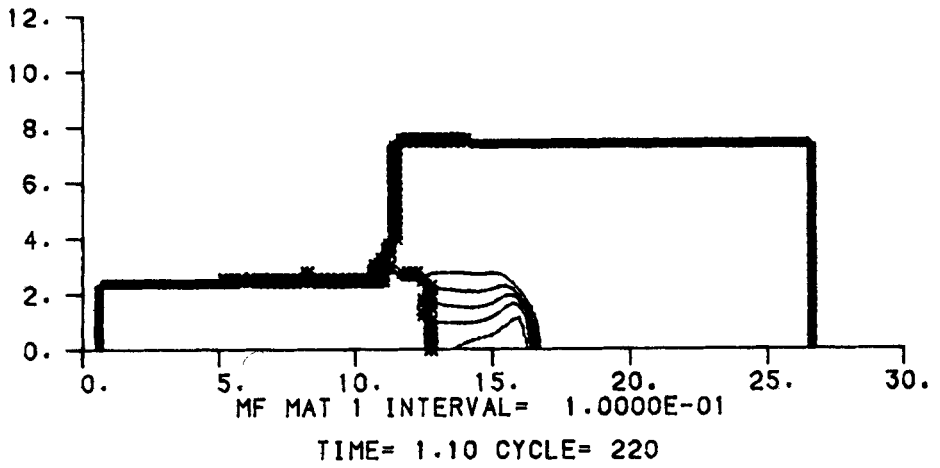


FIGURE 10

Sequence of Mass Fraction Contour Plots for the Supercritical Impact of a "Rectangular" Cross-Section Steel Projectile at 1.25 km/s

Downloaded At: 14:10 16 January 2011

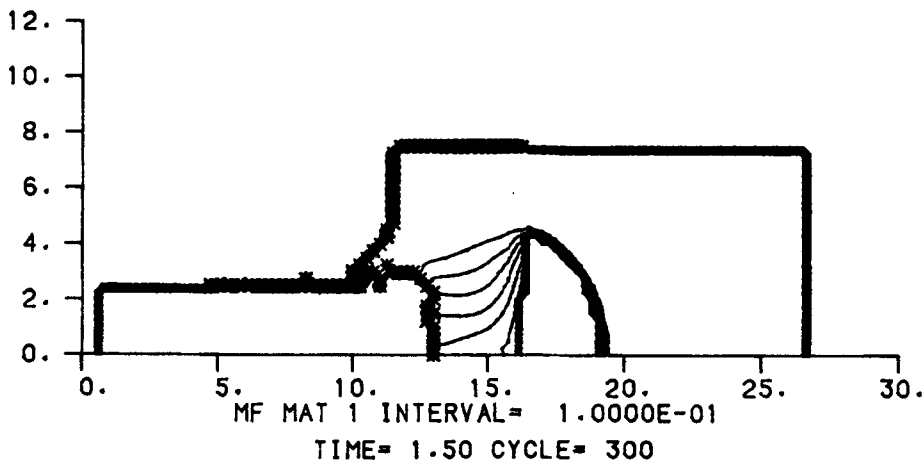
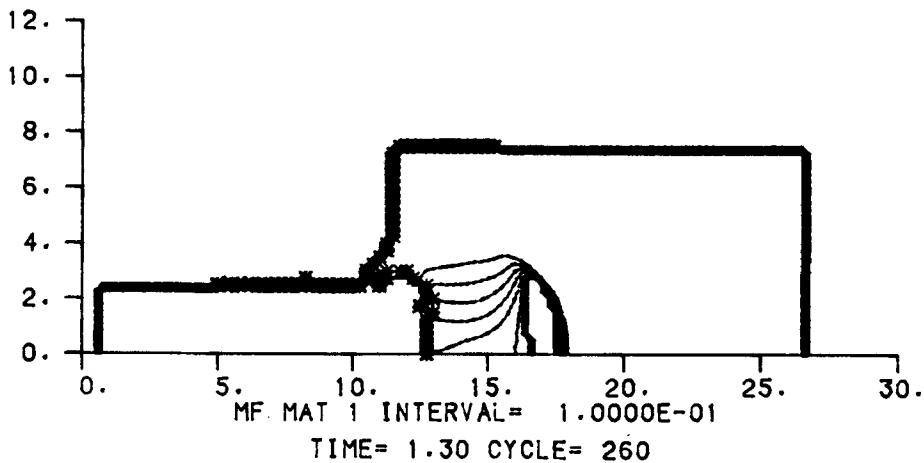


FIGURE 10

(CONT'D)

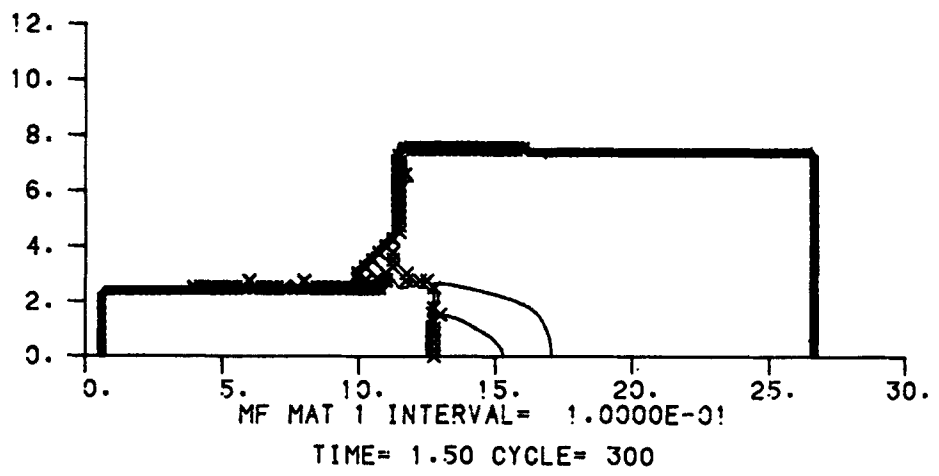
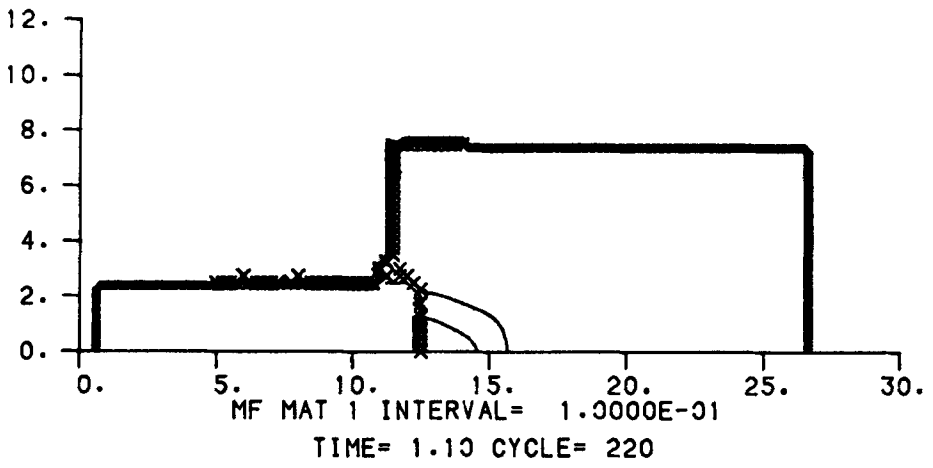


FIGURE 11

Sequence of Mass Fraction Contour Plots for the Subcritical Impact of a "Rectangular" Cross-Section Steel Projectile at 1.1 km/s against Bare Composition-B

Downloaded At: 14:10 16 January 2011

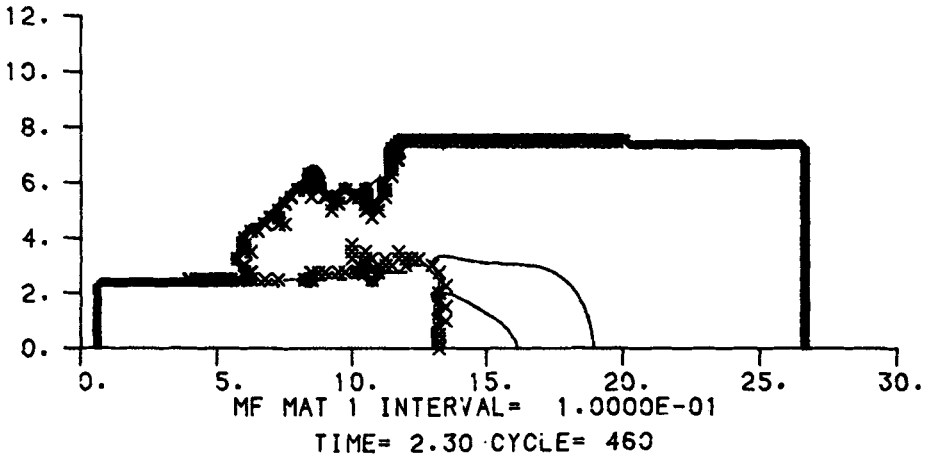
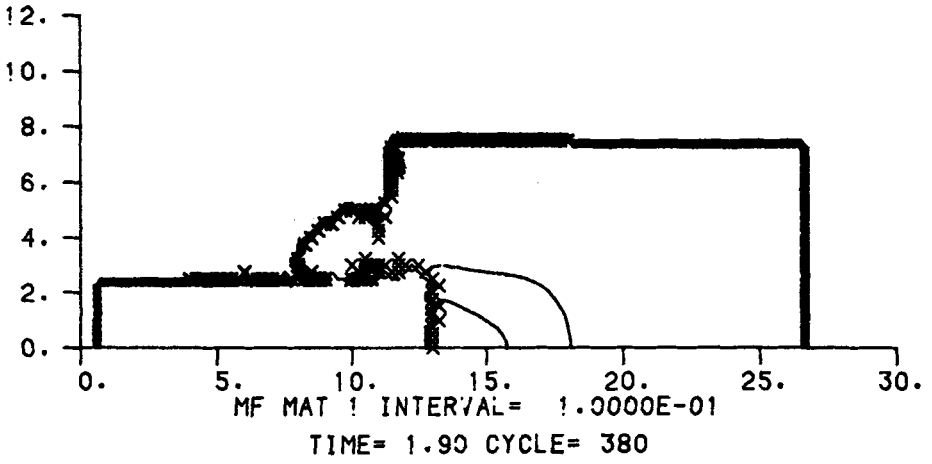


FIGURE 11

(CONT'D)

detonation transition occurs for the cylindrical projectile also.

PROJECTILE IMPACT SHOCK INITIATION OF COVERED COMPOSITION-B
Geometry and Computational Considerations

We have also addressed the related problem of projectile impact of covered comp-B by introducing a steel plate of thickness, h , between the projectile and the explosive. Projectile diameters of 6, 8, and 10 mm and cover plates of 1/8, 1/4, 1/2, and 3/4 as thick as the diameter in each case were considered. Other geometrical considerations are as described for the bare charge problem. The axisymmetric computational grids are described in Table 4.

Downloaded At: 14:10 16 January 2011

TABLE 4. Data for 2DE Computational Grids - Covered Charges

d	h/d	$\Delta r, \Delta z$	I	J	t	N
(mm)		(mm)			(μs)	
6	1/8	0.15	45	100	0.004	400
6	1/4	0.15	45	100	0.004	600
6	1/2	0.15	45	100	0.004	650
6	3/4	0.15	45	100	0.004	700
8	1/8	0.20	45	100	0.005	450
8	1/4	0.20	45	100	0.005	600
8	1/2	0.20	45	110	0.005	800
8	3/4	0.20	45	120	0.005	800
10	1/8	0.25	45	100	0.005	500
10	1/4	0.34	55	125	0.008	700
10	1/2	0.20	55	140	0.005	750
10	3/4	0.20	55	140	0.005	800

Results

Flow Field Observations. Typical results are shown in the mass fraction contour plot sequence of Figure 12. This is for the 1.75 km/s impact of an 8 mm diameter projectile against a comp-B target protected by a 4 mm thick cover plate. In general, the flow fields were quite similar to those observed in the bare charge cases. Only the case of the 6 mm diameter projectile with the 1.5 mm thick cover plate showed the small diameter effect observed in the bare charge problems. In this case we observed a quick shock to detonation transition followed by

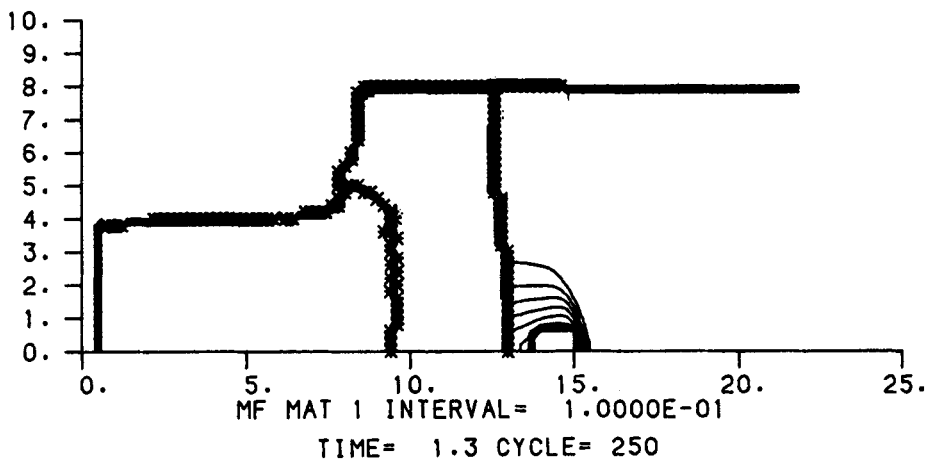
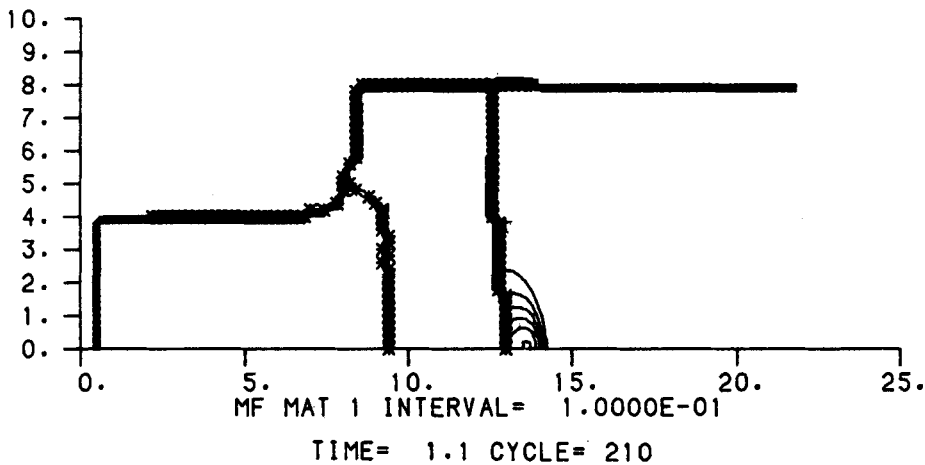


FIGURE 12

Sequence of Mass Fraction Contour Plots for the Supercritical Impact of an 8 mm Diameter Steel Projectile at 1.75 km/s against a Composition-B Target Protected by a 4 mm Thick Steel Cover Plate

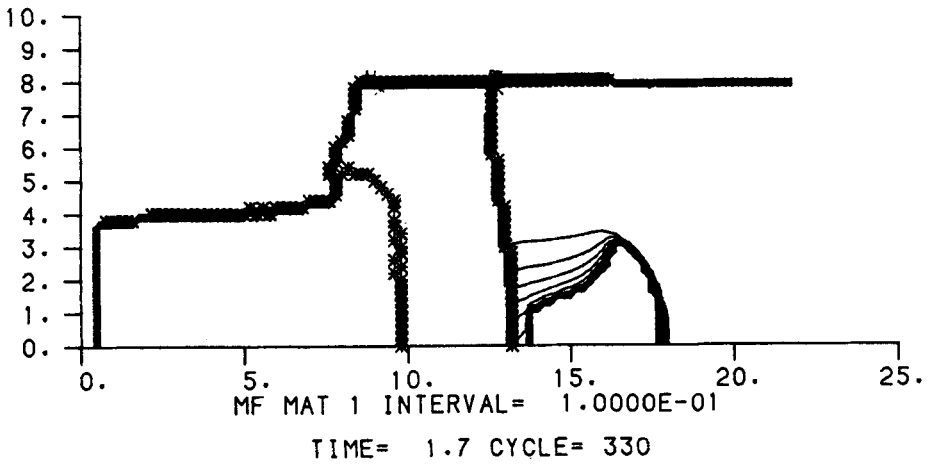
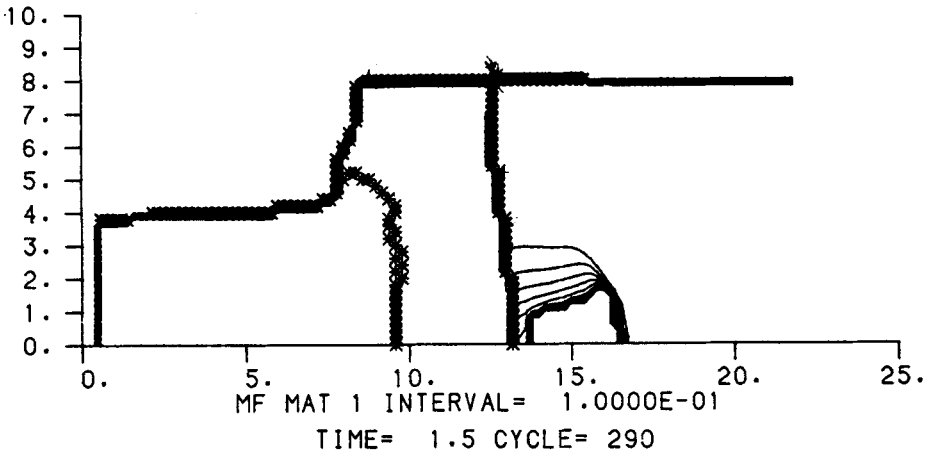


FIGURE 12

(CONT'D)

quenching. This is shown in Figure 13. However, we did not consider quite as small projectiles in the covered charge problem. With the thickest cover plate ($h/d=3/4$) the rarefaction was observed to overtake the shock completely within the cover plate before propagating into the explosive. In these cases, detonation, when produced, develops at a decaying shock wave and the critical velocity is higher than might be anticipated.

Determination of Critical Impact Velocity and Comparison with Experimental Data. A limited quantity of covered comp-B experimental data for comparison is available. This includes the early results of Slade and Dewey as well as some more recent results obtained by Howe⁹ for projectile attack against 105 mm ammunition. The Jacobs-Roslund formula for covered explosive suggests that the product of critical velocity and square root of projectile diameter depends only on the h/d ratio. Thus, in Figure 14 we have plotted our 2DE results together with the aforementioned experimental data in the $V*d^{1/2}$ - h/d plane. The 2DE predictions appear independent of projectile diameter but do not produce a straight line in this plane. They agree quite closely with the Howe results at the two smaller h/d ratios and not as well with the Slade and Dewey experiments. This is a curious result since the Slade and Dewey experiments, with relatively thin cover plates, almost certainly produce shock initiation and Howe has interpreted his observed initiations

with thicker shell casings as due to a shear mechanism. The matter is further complicated by the fact that the 2DE computations do agree with the Slade and Dewey bare charge results. A straight line has been fitted through the 2DE and Howe results for $0.2 < h/d < 0.6$. Both the experimental and theoretical results lie above the straight line for $h/d > 0.6$ and do not agree closely with one another.

If the 2DE results for covered charges are correct, then the Slade and Dewey results become suspect and Howe's experimental initiations must be due to shock. The difference observed at the larger h/d values would then indicate lower computational accuracy, possibly due to the inadequacy of the Forest Fire model when the rarefaction immediately follows the initiating shock. It appears more likely, however, that the Slade and Dewey data are correct. Then, the 2DE results must be in error and Howe's initiations may properly be attributed to a mechanism other than shock.

SUMMARY

Our computational study of projectile impact shock initiation of composition-B revealed details of the flow fields produced and provided predictions of critical impact velocities for both bare and covered explosive targets.

For bare charges, we observed two different mechanisms by which the critical velocity is determined. For impacts by projectiles of sufficiently large diameter initiation occurs as

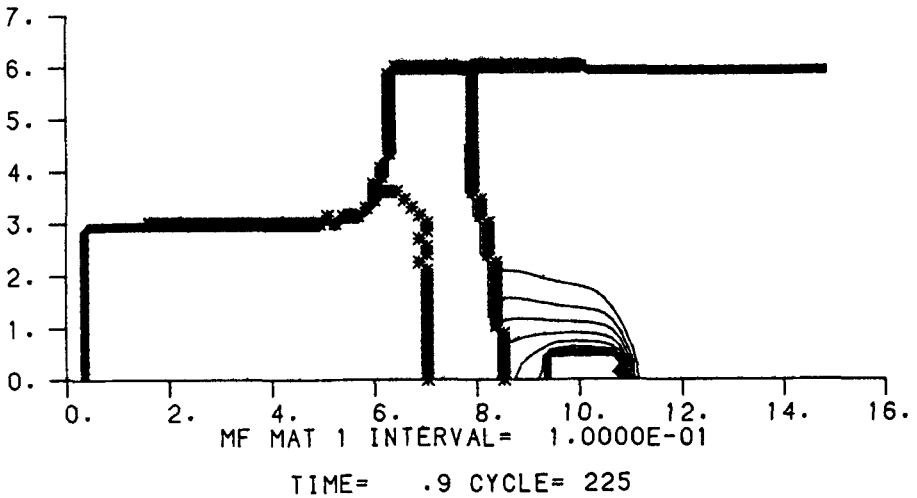
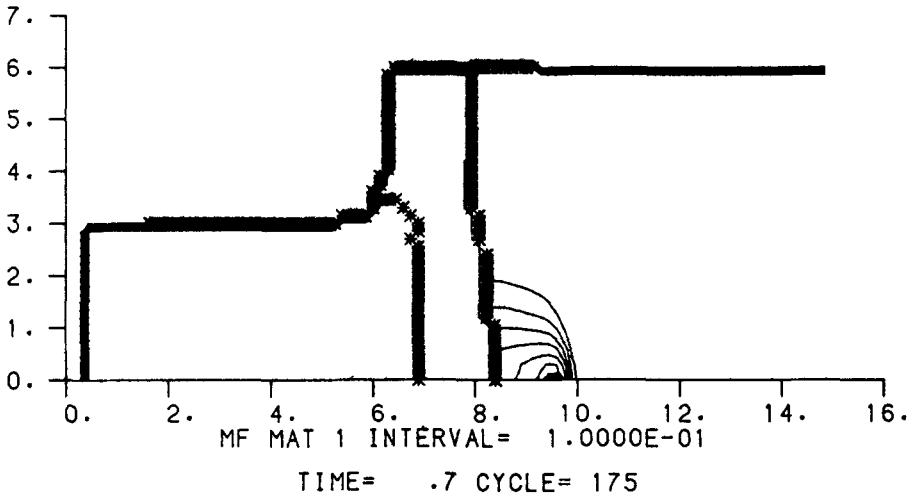


FIGURE 13

Sequence of Mass Fraction Contour Plots for the Subcritical Impact of a 6 mm Diameter Steel Projectile at 1.4 km/s against a Composition-B Target Protected by a 1.5 mm Thick Steel Cover Plate

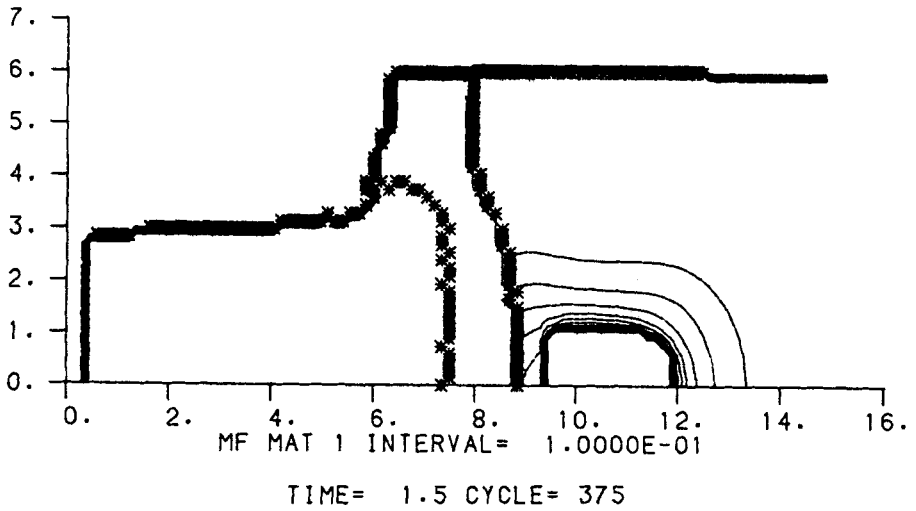
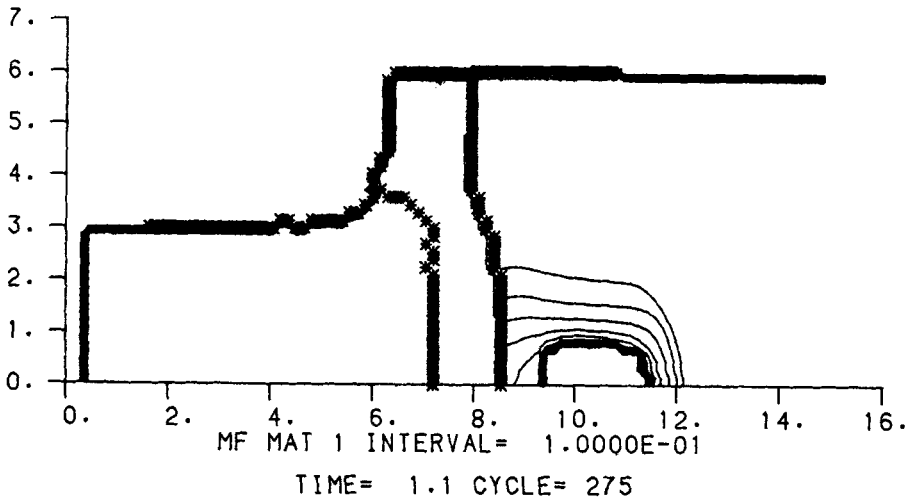


FIGURE 13

(CONT'D)

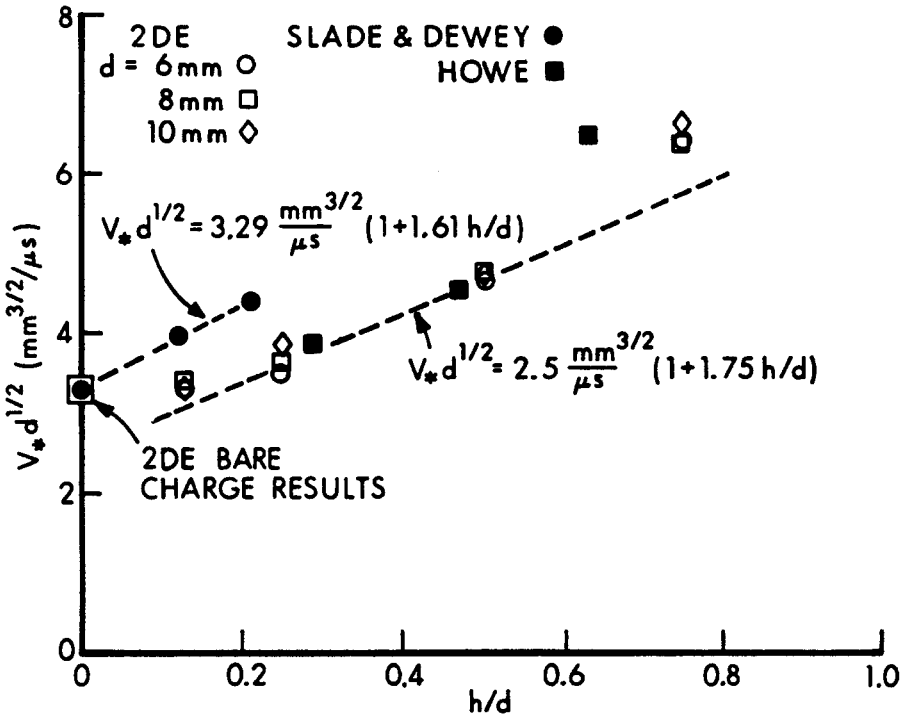


FIGURE 14

Correlation of $V_*d^{1/2}$ with h/d - Comparison of 2DE Predictions with Experimental Data

the impact induced shock wave builds to detonation by reinforcement due to burning behind the shock. For smaller diameter, high velocity projectiles, we saw that detonation or near detonation breaks out immediately on impact, but may be quenched by the ensuing rarefactions. We found that 2DE predicted the critical velocity accurately, We also checked $\int p^2 dt$ values along the initiation threshold and found them to be relatively constant. We compared the shock to detonation transition paths to the Pop-plot for comp-B and found them to agree in the case of a planar shock buildup but not in the case of projectile impact, for which multiple paths to detonation were observed. We also simulated the special projectile geometries considered by Moulard, and found that 2DE provided a qualitative explanation of his observations.

In the case of covered projectiles we found flow fields similar to the bare charge case. The thickest cover plates allowed the rarefaction to overtake the shock before they entered the explosive and significantly raised the critical velocity. The predicted initiation thresholds agree with Howe's results but not with Slade and Dewey's.

REFERENCES

1. D. C. Slade and J. Dewey, "High-Order Initiation of two Military Explosives by Projectile Impact", Ballistic Research Laboratory Report No. 1021, July 1957.

2. S. M. Brown and E. G. Whitbread, "The Initiation of Detonation by Shock Waves of Known Duration and Intensity", *Les Ondes de Detonation*, C.N.R.S. No. 109, pp. 69-80, Paris, 1962.
3. L. A. Roslund, J. W. Watt and N. L. Coleburn, "Initiation of Warhead Explosives by the Impact of Controlled Fragments. I Normal Impact", Naval Ordnance Laboratory Technical Report NOLTR-73-124, August 1974.
4. K. L. Bahl, H. C. Vantine and R. C. Weingart, "The Shock Initiation of Bare and Covered Explosives by Projectile Impact", Seventh Symposium (International) on Detonation, June 1981, pp. 325-335.
5. C. L. Mader and G. H. Pimbley, "Jet Initiation and Penetration of Explosives", *Journal of Energetic Materials*, Vol. 1, No. 1, 1983, pp 1-44.
6. J. D. Kershner and C. L. Mader, "2DE, A Two-Dimensional Continuous Eulerian Hydrodynamic Code for Computing Multicomponent Reactive Hydrodynamic Problems", Los Alamos Scientific Laboratory Report LA-4846, March 1972.
7. H. Moulard, "Critical Conditions for Shock Initiation of Detonation by Small Projectile Impact", Seventh Symposium (International) on Detonation, June 1981, pp. 316-324.

8. J. Starckenberg, Y. K. Huang and A. L. Arbuckle, "A Two-Dimensional Numerical Study of Detonation Propagation Between Munitions by Means of Shock Initiation", BRL Report ARBRL-TR-02522. September 1983.
9. P. M. Howe, personal communication.